Extracted By Dr.S.Aravamudhan from URL:=
http://www.ncbi.nlm.nih.gov/pmc/articles/PMC2933656/?tool=pubmed

ON BLOCH SIEGERT SHIFT & its CURRENT APP:ICATIONS

B$_1$ Mapping by Bloch-Siegert Shift

Laura I. Sacolick,[1] Florian Wiesinger,[1] Ileana Hancu,[2] and Mika W. Vogel[1]
[1]Imaging Technologies Lab, GE Global Research, Garching b. Munchen, Germany
[2]Imaging Technologies Lab, GE Global Research, Niskayuna, New York, USA
Correspondence to: Laura Sacolick, General Electric Global Research, Freisinger Landstrasse 50, Garching b. Munchen 85748, Tel: +49 (0) 89 5528 3727, Email: laura.sacolick@ge.com
▸The publisher's final edited version of this article is available at Magn Reson Med

Abstract
A novel method for B$_1^+$ field mapping based on the Bloch-Siegert shift is presented. Unlike conventionally applied double-angle or other signal magnitude-based methods it encodes the B$_1$ information into signal phase, resulting in important advantages in terms of acquisition speed, accuracy and robustness. The Bloch Siegert frequency shift is caused by irradiating with an off-resonance RF pulse following conventional spin excitation. When applying the off-resonance RF in the kHz range, spin nutation can be neglected and the primarily observed effect is a spin precession frequency shift. This shift is proportional to the square of the RF field magnitude B$_1^2$. Adding gradient image encoding following the off-resonance pulse allows one to acquire spatially resolved B$_1$ maps. The frequency shift from the Bloch-Siegert effect gives a phase shift in the image that is proportional to B$_1^2$. The phase difference of two acquisitions, with the RF pulse applied at two frequencies symmetrically around the water resonance is used to eliminate undesired off-resonance effects due to B$_0$ inhomogeneity and chemical shift. In-vivo Bloch Siegert B$_1$ mapping with 25 seconds / slice is demonstrated to be quantitatively comparable to a

21 minute double-angle map. As such this method enables robust, high resolution B_1^+ mapping in a clinically acceptable time frame.

INTRODUCTION

A wide variety of B_1 mapping methods have been developed to date, however no single one has emerged yet in widespread application. B_1 mapping is used in diverse applications in MR-including transmit gain adjustment to produce specific flip angle RF pulses, design of multi-transmit channel RF pulses (1-3), T_1 mapping and other quantitative MRI (4), and chemical shift imaging.

Generally, B_1 mapping methods fall into two classes: signal magnitude, or signal phase-based. The large majority of B_1 mapping methods depend on changes in signal magnitude based on RF flip angle. Existing methods in this category include fitting progressively increasing flip angles (5), stimulated echoes (6), image signal ratios (7-10), signal null at certain flip angles (11), and comparison of spin echo and stimulated echo signals (12).

These methods suffer from combinations of the following problems: T_1 dependence, long acquisition times-mainly from acquiring many images, and/or a long TR to mitigate the T_1 dependence, inability to use some of these methods with slice-selection, or in a multi-slice acquisition, inaccuracy over a large range of B_1 especially at low flip angles or flip angles close to 90° or 180°, and large RF power deposition in the case of B_1 mapping sequences based on large flip angles or reset pulses to mitigate the T_1 dependence.

There are far fewer phase-based B_1 mapping methods. One method by Morrell uses the phase accrued from a 2α - α flip angle sequence to determine B_1 (13). This method has the same long TR requirement as the signal magnitude-based sequences, although it is effective and more accurate over a larger range of flip angles than a double-angle signal magnitude-based B_1 map (14). A very different phase-based approach was proposed by J.Y. Park and M. Garwood, where they utilize the B_1-dependent phase produced by adiabatic hyperbolic secant half- and full-passage pulses (15). This method nicely eliminates the problems of T_1 and B_0 dependence, however SAR is a significantly limiting factor in applying this clinically at high field.

Here, we describe a novel phase-based B_1 mapping method based on the Bloch-Siegert shift(16). This Bloch-Siegert shift is utilized to create a $|B_1|$-dependent signal phase. The resulting B_1 mapping method is shown here to be robust to TR, T_1 relaxation, flip angle, chemical shift, background field inhomogeneity, and magnetization transfer. Because of this insensitivity, accurate Bloch-Siegert based B_1 maps can be acquired very quickly with a short TR.

THEORY

The term Bloch-Siegert shift has been used to describe the effect where the resonance frequency of a nucleus shifts when an off-resonance RF field is applied (16,17). This effect is an additional contribution to the static B_0 field that arises from the off-resonance component of the RF field. In the case where RF is applied either far enough off-resonance and/or with a pulse shape such that it does not cause spin excitation, the spins experience a change in precession frequency without excitation (18). The spin precession frequency shifts away from the off-resonance irradiation, and is dependent on the magnitude of the B_1 field, and the difference between the spin resonance and RF frequency ω_{RF}.

Figure 1 shows the effective B_1 field in the RF rotating frame (B_1^{eff}) when the RF is applied off-resonance at frequency ω_{RF}. The frequency difference between spin precession and the RF frequency can be visualized as a constant magnetic field along z. In this rotating frame the B_1^{eff} field is constant, and is given by Eqn 1:
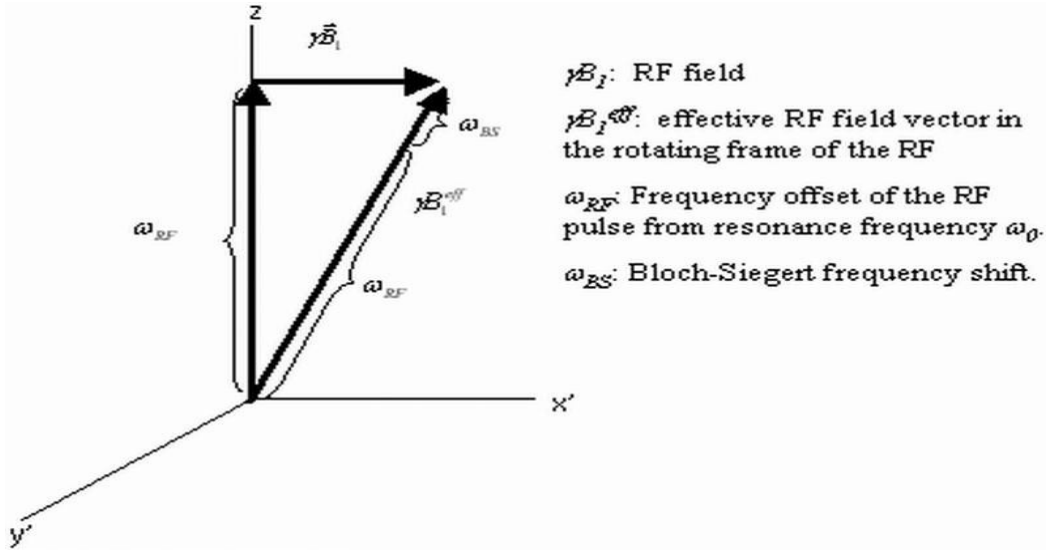
$$\gamma B_1^{eff} = \sqrt{\omega_{RF}^2 + \gamma B_1^2}$$ [1]

For a large off resonance $\omega_{RF} \gg \gamma B_1$ this results in the component ω_{BS} of the B_1^{eff} field vector which is a small constant field approximately along the main magnetic field axis. This additional field constitutes the Bloch-Siegert shift and results in the spin precession frequency shift coming from off-resonance RF irradiation.
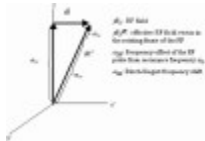
Figure 1

B_1 field in the rotating frame of the RF. The frame rotates at frequency $\omega_0 + \omega_{RF}$. In this frame, the B_1 field is static, where as the spins rotate at ω_{RF}. The Bloch-Siegert frequency shift ω_{BS} is a constant field in this (more ...)

$\gamma\vec{B_1}$: RF field

γB_1^{eff}: effective RF field vector in the rotating frame of the RF

ω_{RF}: Frequency offset of the RF pulse from resonance frequency ω_0.

ω_{BS}: Bloch-Siegert frequency shift.

A simple analytical relationship for the Bloch-Siegert shift ω_{BS} can be derived from Figure 1. Under the assumption of large, relative off-resonance:

$$\omega_{RF} \gg \gamma B_1 \qquad\qquad [2]$$

a trigonometric identity can by used to solve for ω_{BS} according to:

$$\left(\omega_{BS}+\omega_{RF}\right)^2=\omega_{RF}^2+\left(\gamma B_1\right)^2 \qquad\qquad [3]$$

$$\omega_{BS}=\frac{\left(\gamma B_1\right)^2}{2\omega_{RF}} \qquad\qquad [4]$$

This derivation is described in detail by Ramsey in a theoretical paper in Phys Rev. 1955 ([17]). This paper first describes the case dealt with here where a single non-resonant frequency is applied, and later deals more generally with irradiation at multiple non-resonant frequencies.
In practical application, the Bloch-Siegert shift has been used for determining the magnitude of a B_1 decoupling field in solid state spectroscopy ([19],[20]). However to the best knowledge of the authors this has never been applied in MR imaging.
The Bloch-Siegert shift can be applied to B_1 field mapping as follows: An off-resonance RF pulse of frequency ω_{RF} is applied immediately after excitation in an imaging sequence. The RF pulse shape and frequency is chosen such that it does not excite spins in the sample. The frequency shift of spins during the off-resonant RF pulse results in a phase shift in the image that can be used to determine the spatial B_1 magnitude. The phase shift φ_{BS} due to the Bloch-Siegert shift is given by:

$$\varphi_{BS} = \int_0^T \omega_{BS}(t) = \int_0^T \frac{(\gamma B_1(t))^2}{2\omega_{RF}(t)} dt \tag{5}$$

The expected phase shift can be calculated from Eqn. 5 for any arbitrary pulse $B_1(t)$ with constant or time dependent frequency offset $\omega_{RF}(t)$.

The relationship between Bloch-Siegert phase shift and the peak B_1 of a generalized RF pulse is given by Eqn. 6:

$$\varphi_{BS} = B_{1,peak}^2 \int_0^T \frac{(\gamma B_{1,normalized}(t))^2}{2\omega_{RF}(t)} dt = B_{1,peak}^2 \times K_{BS} \tag{6}$$

$$B_1(t) = B_{1,peak} * B_{1,normalized}(t) \tag{7}$$

K_{BS} is a constant that describes the phase shift (radians/gauss^2) for a given RF pulse. For example: for a hard pulse, 4 kHz off resonance, $K_{BS} = 14.23$ radians/gauss^2/msec. $B_{1,peak}$ is the magnitude of the maximum point in the RF waveform $B_1(t)$.

Phase-based methods usually require taking the difference of two scans to remove additional, undesired phase effects in the image. The difference in phase between the two scans gives the Bloch-Siegert phase shift, removing transmit excitation and receive phases, other sequence related phase, and the phase shift from off-resonance B_0. All these phase factors are the same in both scans. Acquiring two scans- one with the RF pulse at $+\omega_{RF}$, and one at $-\omega_{RF}$ enables one to calculate B_1. Applying the off-resonance RF symmetrically around the water peak removes the B_0-inhomogeneity and chemical shift dependence of the Bloch-Siegert shift as well. For off-resonance spins precessing at frequency $\omega_0 + \omega_{B0}$, Eqn. 4 for the Bloch Siegert frequency shift becomes:

$$\omega_{BS} = \frac{(\gamma B_1)^2}{2(\omega_{RF} + \omega_{B0})} \tag{8}$$

By a 2nd order Taylor expansion, assuming $\omega_{B0} \ll \omega_{RF}$:

$$\omega_{BS} = \frac{(\gamma B_1)^2}{2(\omega_{RF} + \omega_{B0})} \approx \frac{(\gamma B_1)^2}{2\omega_{RF}} - \frac{(\gamma B_1)^2 \omega_{B0}}{2\omega_{RF}^2} + O\left(\omega_{B0}^2\right) \tag{9}$$

The Bloch-Siegert phase shift of a spin at B_0 offset of ω_{B0} is given by:

$$\varphi_{BS} \approx \int_0^T \frac{(\gamma B_1(t))^2}{2\omega_{RF}(t)} dt - \int_0^T \frac{(\gamma B_1(t))^2 \omega_{B0}}{2\omega_{RF}^2} dt + O\left(\omega_{B0}^2\right) \tag{10}$$

The ω_{B0} dependent term drops out when one takes the phase difference between two scans with the off-resonance pulse at symmetric +/− ω_{RF} frequencies. The result is a phase shift that is up to first order independent of off-resonance frequency.

The percentage error in B_1 calculated from the phase difference of two scans with off-resonance RF applied at +/− ω_{RF}, where there is a B_0 offset of ω_{B0} is given by Eqn's 11 and 12:

$$\text{error}\left(\varphi_{BS}\right) = \frac{\int_0^T \left(\dfrac{(\gamma B_1(t))^2}{2\left(\omega_{RF}(t)+\omega_{B0}\right)} + \dfrac{(\gamma B_1(t))^2}{2\left(\omega_{RF}(t)-\omega_{B0}\right)} \right) dt}{\int_0^T \dfrac{(\gamma B_1(t))^2}{\omega_{RF}(t)} dt} \qquad [11]$$

$$\text{error}\left(B_1\right) = 100\% \times \sqrt{\frac{\text{error}\left(\varphi_{BS}\right)}{K_{BS}}} \qquad [12]$$

This percentage error in B_1 calculation as a function of B_0 offset is shown in Figure 2. The error is shown for RF pulses at off-resonance frequencies 2, 4, and 8 kHz, over a range of +/− 1 kHz B_0 inhomogeneity.
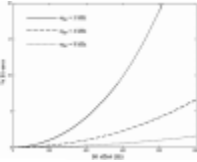
Figure 2
Percentage error in B_1 calculation as a function of B_0 offset over a range of 1 kHz. The error is calculated from Eqns. 11 and 12, for RF pulses at off-resonance frequencies of 2, 4, 8 kHz.
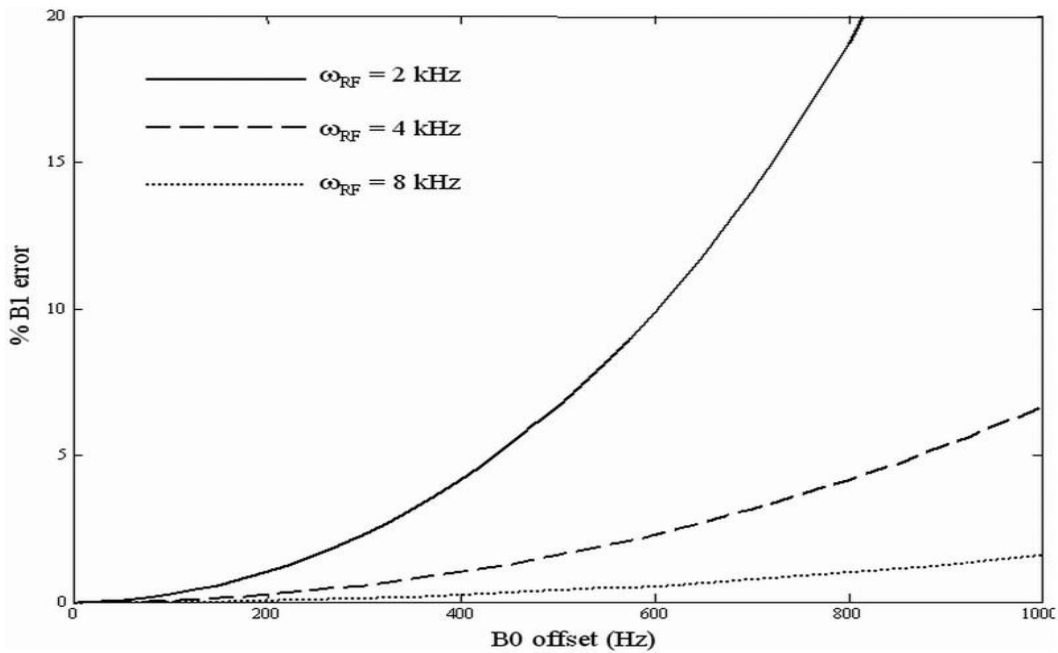
METHODS

The sequences in Figure 3 were implemented on a 3 Tesla GE DVMR scanner, (GE Healthcare, Milwaukee, WI, USA). 15 human subjects were studied in accordance with institutional review board guidelines for in-vivo research. All subjects provided informed consent. A basic gradient echo sequence was modified by including an off-resonance Fermi pulse immediately following excitation. A basic spin echo sequence was modified by including two Fermi pulses, applied around a refocusing pulse. All gradient echo images shown in this work were acquired with an 8 msec Fermi saturation pulse, and frequency offsets of $\omega_{RF} = +/- 4$ kHz relative to water. All spin echo B_1 maps were acquired with two 6 msec Fermi saturation pulses, and frequency offsets of $\omega_{RF} = +/- 4$ kHz relative to water. Figure 4 shows the 8 msec Fermi pulse, and its frequency excitation profile. A frequency profile with minimal on-resonance excitation is necessary to not excite spins in the sample.
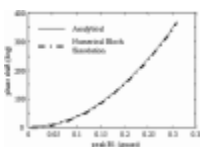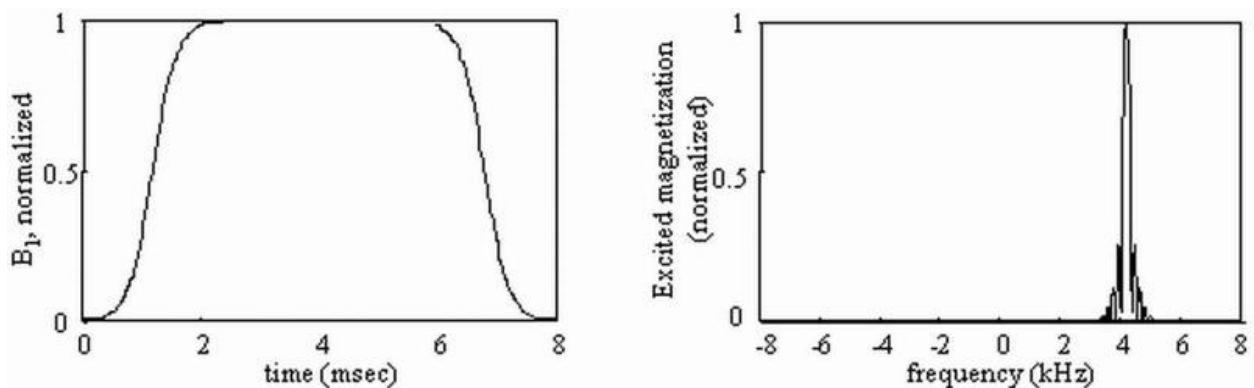
Figure 3

Gradient and spin echo sequences, modified for B_1 mapping. The gradient echo sequence has an 8 msec off-resonance Fermi pulse at off-resonance frequency ω_{RF} following excitation. The spin echo sequence has two 6 msec off-resonance Fermi pulses. (more ...)
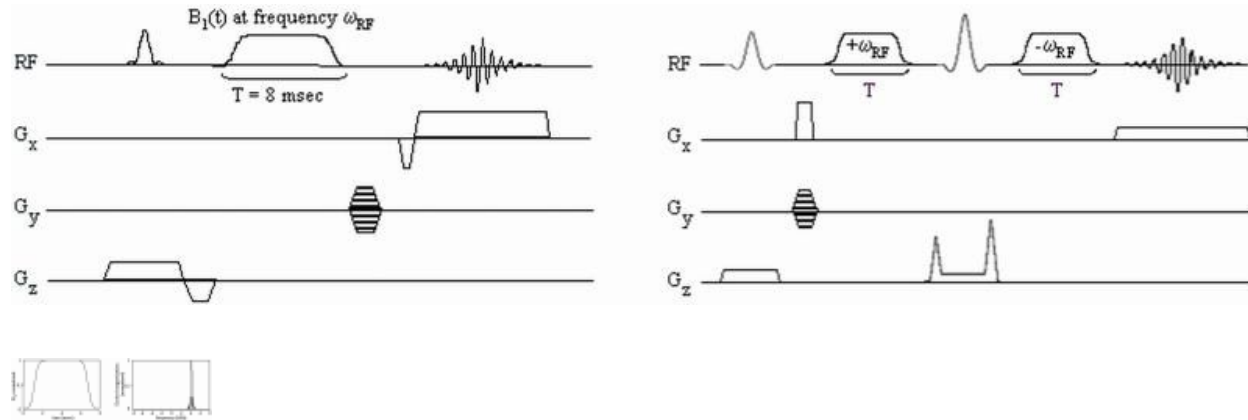
Figure 4

Normalized $B_1(t)$ and corresponding frequency excitation profile for an 8 msec Fermi pulse, and $\omega_{RF} = 4$ kHz.

For the 8 msec 4 kHz off resonance Fermi pulse used in the gradient echo experiments described here, $K_{BS} = 74.01$ radians/gauss^2. For the 6 msec 4 kHz off resonance Fermi pulse used in the spin echo experiments described here, $K_{BS} = 55.26$ radians/gauss^2. The spin echo sequence contains two 6 msec Fermi pulses for a total K_{BS} for the sequence of 110.52 radians/gauss^2. The relationship between phase shift and $B_{1,peak}$ is shown in Figure 5 for the 8 msec Fermi pulse. Also shown is a comparison between the phase shift predicted by the analytical expression in Eqn. 6 and the phase shift predicted by numerical Bloch simulation of this off-resonance pulse.
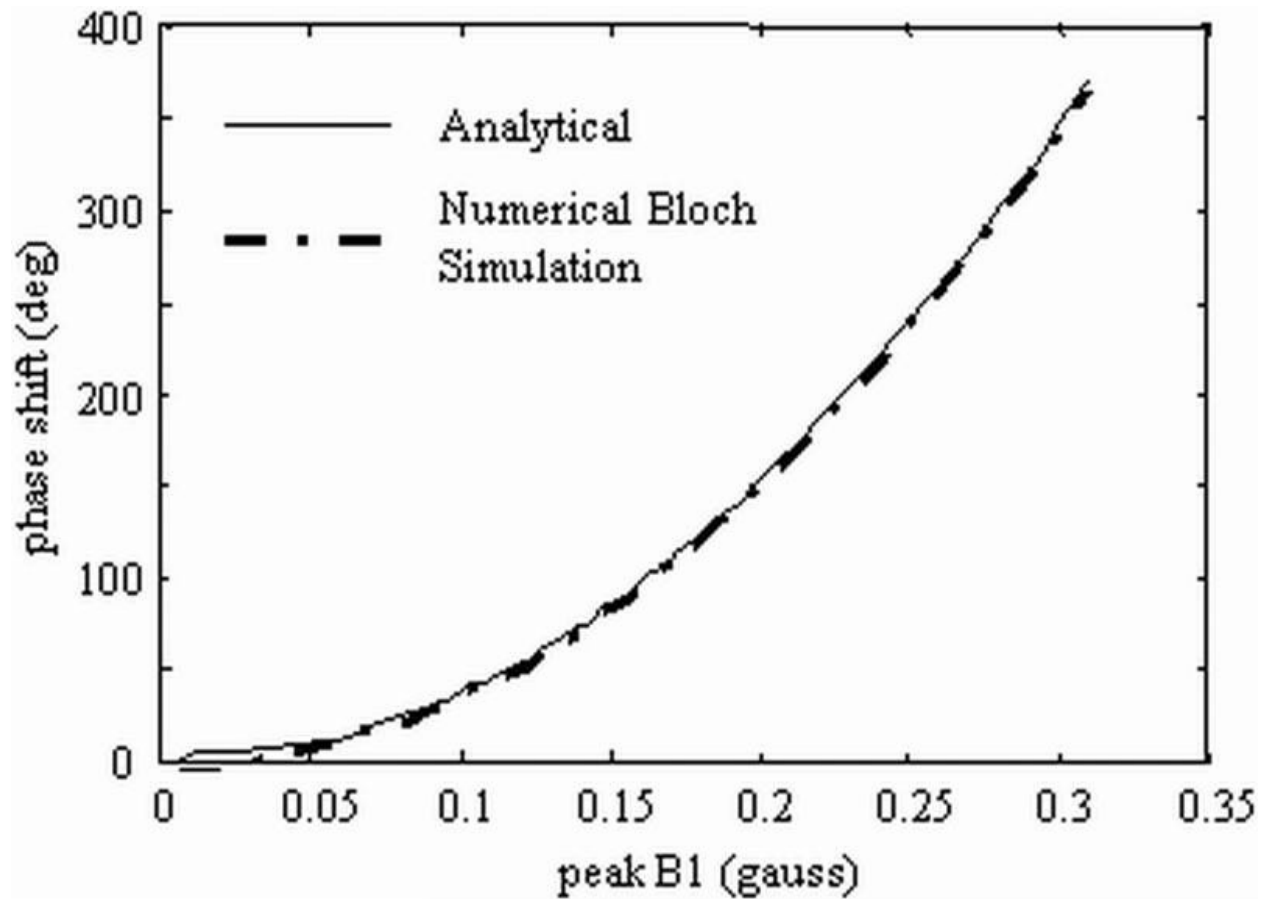
Figure 5

Phase shift φ_{BS} vs. $|B_1|$ for an 8 msec Fermi pulse at 4 kHz. Simulated by the analytical expression of Eqn. 6, and numerical Bloch simulation.
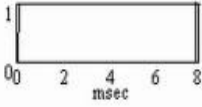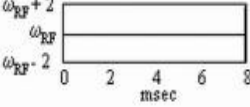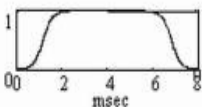
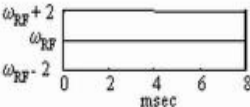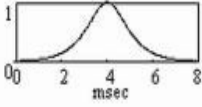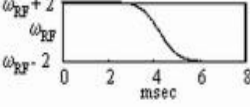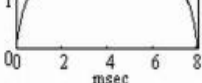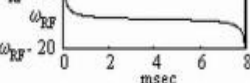The Fermi RF pulse is used regularly for magnetization transfer preparation- which has similar RF pulse requirements as our case here (21,22). The relationship between phase shift and $B_{1,peak}$ can be calculated similarly for any arbitrary RF pulse. Figure 6 shows a comparison of K_{BS} for four choices of RF pulses: the hard pulse, Fermi, and adiabatic sech/tanh, and tanh/tan pulses (23). Also shown is a comparison of the width of the frequency band that contains 99% percent of spin excitation for these pulses.

Figure 6

Comparison of four RF pulses, all of 8 msec pulse length, at 4 kHz off-resonance, relative to water. The hard pulse, Fermi, adiabatic hyperbolic secant (with a time varying frequency sweep $\omega_{RF}(t)$ of +/−2kHz around 4 kHz), and the adiabatic (more ...)

Pulse Type	$B_1(t)$ (normalized)	$\omega_{RF}(t)$ (kHz)	K_{BS} (radians/gauss^2) 8 msec, 4 kHz pulse	Freq. band (kHz) containing 99% of spin excitation
Hard pulse			113.86	37.3
Fermi			74.01	2.1
Hyperbolic secant			38.03	2.3
Adiabatic tanh/tan			101.58	11.2

RESULTS

Gradient echo Bloch-Siegert B_1 maps and double angle maps were acquired from a silicon oil phantom, and a saline phantom with three inner subcompartments filled with milk to assess sensitivity of this method to chemical shift and to magnetization transfer. A GE birdcage transmit/receive head coil was used for RF transmission and reception.

Figure 7a shows a double angle B_1 map of the silicon oil phantom. The two gradient echo images were acquired with TE = 10 msec, TR = 5 sec, flip angles $\alpha = 60°$, $2\alpha = 120°$, slice thickness 1 cm,

in plane resolution 128×128. The flip angle map for the 60° image was calculated by ([24](#)):

$$B_1^{\text{flip angle}} = \arccos\left(\frac{S_{2\alpha}}{2S_\alpha}\right) \quad\quad\quad [13]$$

where $S_{2\alpha}$ and S_α are the signal magnitudes of the 2x and 1x flip angle images. The B_1 map calculated for the 60° flip angle RF pulse is shown here for comparison with the Bloch-Siegert B_1 maps. [Figure 7b](#) shows two Bloch-Siegert B_1 maps taken with TE = 15 msec, and TR of 70 and 2000 msec, which demonstrate lack of TR-dependence. [Figure 7c](#) shows the percent difference between the double angle map and the 70 msec TR Bloch-Siegert map. These match to within 2%.
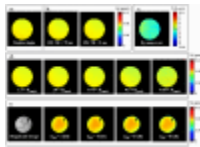
[Figure 7](#)

a. Double angle B_1 map, calculated from two scans acquired with a 3.2 msec sinc pulse having flip angles of $\alpha = 60°$, $2\alpha = 120°$, TE = 10 msec, TR = 5 sec. Slice thickness = 1 cm, 128×128 resolution. **b.** Gradient echo [(more ...)](#)
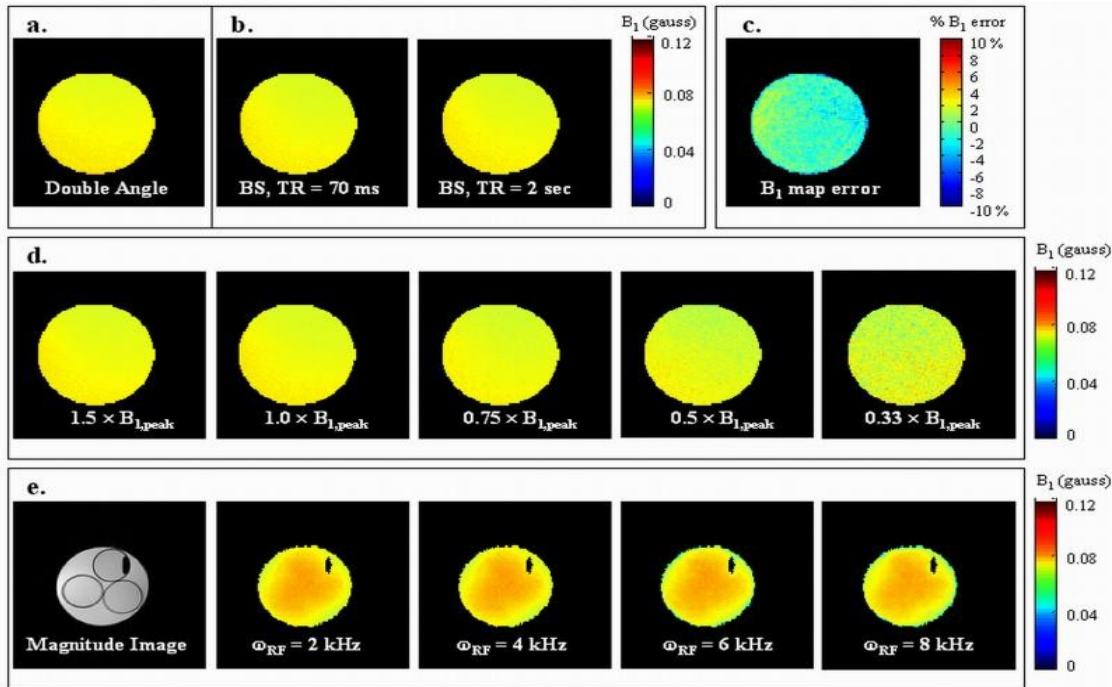

[Figure 7d](#) shows Bloch-Siegert B_1 maps as a function of peak B_1 power. Four Bloch-Siegert B_1

maps were acquired with $B_{1,peak}$ = 0.11, 0.073, 0.055, 0.037, 0.024 gauss. $B_{1,peak}$ was controlled by scaling the exciter output by 1.5, 1.0, 0.75, 0.5, 0.33. The B_1 maps are scaled by these factors for easier comparison.

Figure 7e shows Bloch-Siegert maps of the saline/milk phantom acquired with the 8 msec Fermi pulse at off-resonance frequencies of 2, 4, 6, and 8 Hz relative to the water resonance. No effect of chemical shift or magnetization transfer is evident in the milk or water compartments.

The B_1 maps in Figure 7d and e were acquired with TR = 70 msec. Total scanning times were 21.3 min. for the double angle map, and 18 sec. for the Bloch-Siegert maps.
This was repeated in-vivo in the brain, sagittal orientation, with a GE birdcage transmit/receive head coil (Figure 8). There is a small difference in the magnitude images with the off-resonance pulse (Figure 8a, b.) and without the off-resonance pulse (Figure 8c). This is likely the result of magnetization transfer, however this does not cause any obvious artifacts in the B_1 map. The double angle map in Figure 8d overestimates the B_1 field in the CSF, resulting from the known T_1 dependence of this method and the less than optimal TR of 3 seconds. T_1 dependence is not evident in the Bloch Siegert B_1 map of Figure 8e.
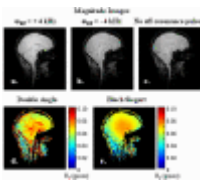
Figure 8

a, b. Magnitude gradient echo images with 8 msec off-resonance Fermi pulse, $\omega_{RF} = +/- 4$ kHz.
c. Same image acquisition, without the off-resonance pulse. **d.** Double angle B_1 map, 128×128,
slice thickness = 0.5 mm, TE = 12 msec, TR (more ...)

Magnitude Images

$\omega_{RF} = + 4$ kHz $\omega_{RF} = - 4$ kHz   No off-resonance pulse

a.   b.   c.

Double Angle   Bloch Siegert

B_1 (gauss) B_1 (gauss)
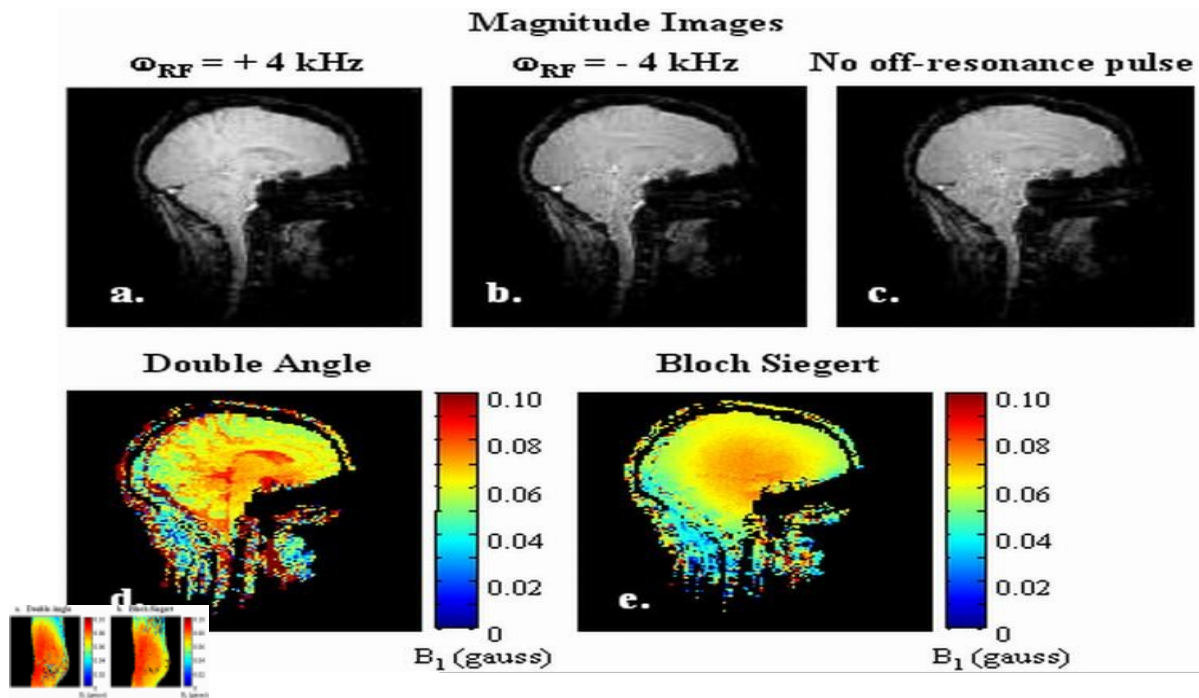
Figure 9

a.   Double angle B_1 map, resolution 128×128, slice thickness = 0.5 mm, TE = 12 msec, TR
= 5 sec. Flip angles $\alpha = 60°$ $2\alpha = 120°$. **b.** Gradient echo Bloch-Siegert map, resolution
128×128, slice thickness = 0.5 (more ...)

a. **Double Angle**   b. **Bloch Siegert**

B_1 (gauss) B_1 (gauss)
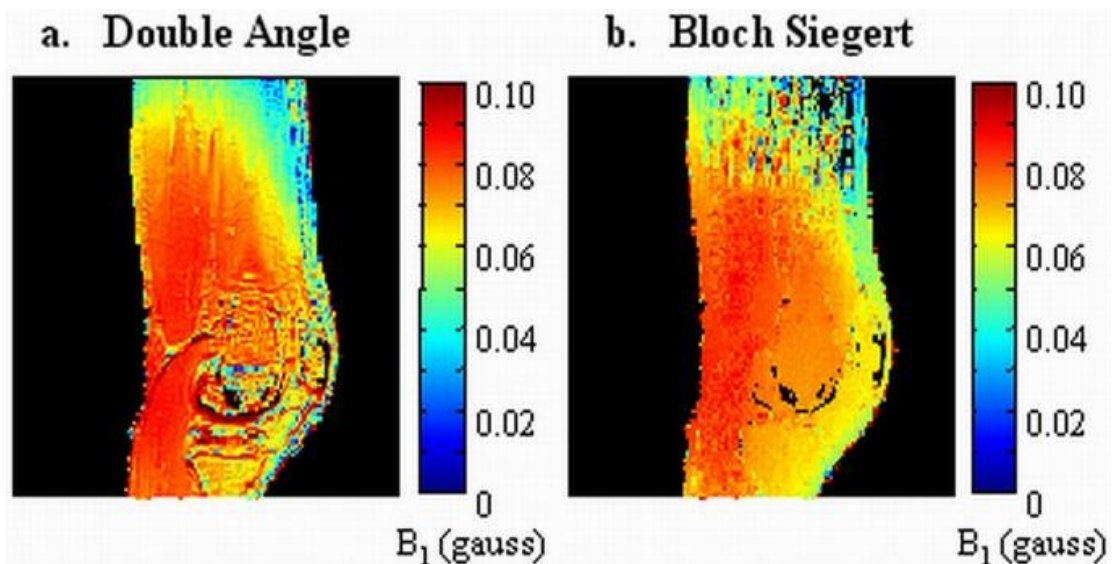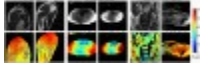
Figure 10

Spin echo Bloch-Siegert B_1 maps, acquired with two 6 msec, $+/-$ 4 kHz off-resonance Fermi pulses, applied symmetrically around a 3.2 msec sinc refocusing pulse. The Fermi pulses had the same peak B_1 as the excitation pulse. TE = 28 msec, TR = 200 (more ...)
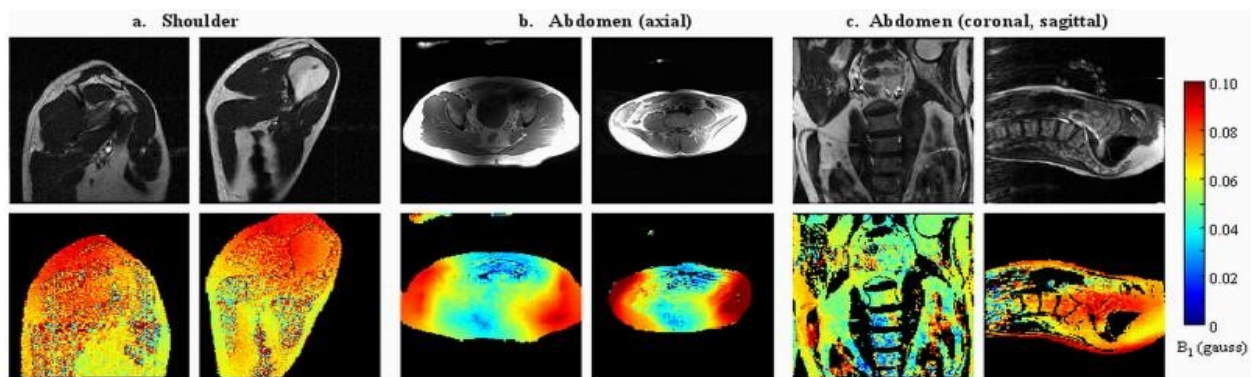
DISCUSSION

The Bloch-Siegert shift gives a fast, accurate, robust, and conceptually straightforward method for measuring B_1 field maps. The Bloch-Siegert shift provides a detectable phase shift to use for B_1 mapping, providing one uses a long enough off-resonance RF pulse with amplitudes compatible with clinical applications. The associated increase in echo time can be afforded for most in-vivo applications. In general, phase sensitive B_1 mapping methods have a significant advantage over signal magnitude based methods in scan time and accuracy over a wide dynamic range of flip angles ([14]). The Bloch-Siegert method in particular is shown here to be insensitive to T_1, TR, chemical shift, magnetization transfer, and inhomogeneous B_0 within a range reasonably expected in vivo.

This method will work with a large variety of off-resonance pulse shapes. The optimal pulse shape for this method would be one that maximizes the integral in [Eqn. 5], but does not directly excite spins in the sample. Several pulse shapes were considered- the hard pulse, adiabatic hyperbolic secant, Gaussian, as well as the Fermi pulse. The latter offered a good choice in terms of maximizing the integral of [Eqn. 5], and minimizing on-resonance excitation.

The Bloch-Siegert phase shift produced by a single off-resonance RF pulse is B_0 dependent. However, the phase difference between two scans with the off-resonance pulse at approximately symmetric frequencies around the on-resonance water peak, is independent of B_0 for $\omega_{B0} \ll \omega_{RF}$. One would choose the RF off-resonance frequency ω_{RF} to satisfy this condition, as well as to avoid on-resonance excitation. The off-resonance frequency ω_{RF} of 4 kHz was chosen for this pulse based on the criteria that the pulse excite <1% of spins within a ±1 kHz range around the center resonance frequency.

The off-resonance Fermi pulse used here to produce the Bloch-Siegert shift is similar to off-resonance RF pulses typically used in a magnetization transfer sequence. There is a magnitude difference between in-vivo images acquired with and without the off-resonance RF pulse that is likely due to magnetization transfer, flow, and motion. There is a small asymmetry in the magnitude of the two images with the off-resonance pulse on either side of the water peak ([25]). However, no phase contribution from the magnetization transfer is evident in any of the in-vivo experiments, or the milk compartment phantom experiments.

Because of the insensitivity of this method to relaxation and TR, one would likely use as short a TR as possible. The SNR of a Bloch-Siegert B_1 map is dependent on the base SNR of the two acquired images, and the phase shift between the images. Scan time in most cases will be limited at lower field by a tradeoff between imaging time and SNR, and at high field ($\geq$ 3 Tesla) by clinical SAR limits.

The Bloch-Siegert phase shift scales with the integrated area of B_1^2, as does SAR. For the gradient echo sequence: All imaging demonstrated here in vivo including acquisitions with TR of 50 msec was within all SAR limits as measured by conventional scanner power monitoring. At 3 Tesla, with a TR of 35 msec, and peak B_1 of 0.2 gauss, we skirt the short term (10 second) SAR limits. However, our in-vivo experiments gave more than adequate signal to noise with peak B_1 = 0.07 gauss and TR of 50 msec. This was well within the long-term SAR limits for continuous scanning. At higher field strengths, one can extend the TR. The spin echo sequence presented here was more SAR intensive, but could be run continuously with a body transmit coil with a peak Fermi pulse B_1 of 0.1 gauss with a TR of 200 msec.

Even at longer TR the time advantage of this method is maintained. This method is fully compatible with EPI, spiral readout, or other imaging acceleration methods, which can additionally reduce scan time and/or SAR.

The Bloch-Siegert shift was used in this work to measure the magnitude of the B_1^+ field, needed in a large number of MR applications. A subclass of these applications may also benefit from knowledge of the phase of the B_1^+ field, or of the receive B_1^- sensitivity. While the B_1^+ phase and the B_1^- profile can not be determined directly from the Bloch-Siegert shift, they may be obtained using information collected in the Bloch-Siegert B_1^+ mapping scans. For example, in a manner similar to the one described by Wang et al. ([26](#)), the B_1^- profile can be obtained using a fast third acquisition with the contrast between tissues minimized, and the B_1^+ map from the Bloch-Siegert shift. B_1 phase is conventionally determined from the phase difference between images where each coil transmits individually. One could similarly take the phase difference between images used for Bloch-Siegert B_1 maps where each coil is used individually for excitation. It may be the case that acquiring B_1 magnitude from the Bloch-Siegert shift, and B_1 receive from a second scan is a beneficial method for parallel transmit applications as well.

REFERENCES

1. Katscher U, Börnert P, Leussler C, van den Brink JS. Transmit SENSE. Magn Reson Med. 2003;49:144–150. [[PubMed](#)]

2. Zhu Y. Parallel excitation with an array of transmit coils. Magn Reson Med. 2004;51:775–784. [[PubMed](#)]

3. Xu D, King KF, Zhu Y, McKinnon GC, Liang ZP. Designing multichannel, multidimensional, arbitrary flip angle RF pulses using an optimal control approach. Magn Reson Med. 2008;59:547–560. [[PMC free article](#)] [[PubMed](#)]

4. Warntjes JB, Leinhard OD, West J, Lundberg P. Rapid magnetic resonance quantification on the brain: Optimization for clinical usage. Magn Reson Med. 2008;60:320–329. [[PubMed](#)]

5. Hornak JP, Szumowski J, Bryant RG. Magnetic field mapping. Magn Reson Med. 1988;6:158–163. [[PubMed](#)]

6. Akoka S, Franconi F, Sequin F, Le Pape A. Radiofrequency map of an NMR coil by imaging. J Magn Reson Imaging. 1993;11:437–441.

7. Stollberger R, Wach P, McKinnon GC, Justich E, Ebner F. RF field mapping in vivo; Proceedings of the 7th Annual Meeting of ISMRM; San Francisco, CA, USA. 1988.p. 106.

8. Maier JK, Glover GH. Method for mapping the RF transmit and receive field in an NMR system. US Patent 5001428. 1991.

9. Cunningham CH, Pauly JM, Nayak KS. Saturated double-angle method for rapid B1+ mapping. Magn Reson Med. 2006;55:1326–1333. [PubMed]

10. Kerr AB, Cunningham CH, Pauly JM, Piel JE, Giaquinto RO, Watkins RD, Zhu Y. Accelerated B1 mapping for parallel excitation; Proceedings of the 15th Annual Meeting of ISMRM; Berlin, Germany. 2007.p. 352.

11. Dowell NG, Tofts PS. Fast, accurate, and precise mapping of the RF field in vivo using the 180° signal null. Magn Reson Med. 2007;58:622–630. [PubMed]

12. Jiru F, Klose U. Fast 3D radiofrequency field mapping using echo-planar imaging. Magn Reson Med. 2006;56:1375–1379. [PubMed]

13. Morrell GR. A phase-sensitive method of flip angle mapping. Magn Reson Med. 2008;60:889–894. [PubMed]

14. Morrell GR, Schabel M. A noise analysis of flip angle mapping methods; Proceedings of the 17th Annual Meeting of ISMRM; Honolulu, HI, USA. 2009.p. 376.

15. Park JY, Garwood M. B1 mapping using phase information created by frequency-moduated pulses; Proceedings of the 16th Annual Meeting of ISMRM; Toronto, Canada. 2008.p. 361.

16. Bloch F, Siegert A. Magnetic resonance for nonrotating fields. Phys Rev. 1940;57:522–527.

17. Ramsey NF. Resonance transitions induced by perturbations at two or more different frequencies. Phys Rev. 1955;100(4):1191–1194.

18. Steffen M, Vandersypen LMK, Chuang IL. Simultaneous soft pulses applied at nearby frequencies. J Magn Reson. 2000;146(2):369–374. [PubMed]

19. Vierkotter SA. Applications of the Bloch-Siegert shift in solid-state proton-dipolar-decoupled 19F MAS NMR. J Magn Reson. 1996;118:84–93.

20. Michal CA, Hastings SP, Lee LH. Two-photon Lee-Goldburg nuclear magnetic resonance: Simultaneous homonuclear decoupling and signal acquisition. J Chem Phys. 2008;128(5):052301. [PubMed]

21. Lin C, Bernstein MA, Gibbs GF, Huston Reduction of RF power for magnetization transfer with optimized application of RF pulses in k-space. Magn Reson Med. 2003;50(1):114–121. [PubMed]

22. Wang Y, Grist TM, Mistretta CA. Dispersion in magnetization transfer contrast at a given specific absorption rate due to variations of RF pulse parameters in the magnetization transfer preparation. Magn Reson Med. 1997;37(6):957–962. [PubMed]

23. Hwang TL, van Zijl PC, Garwood M. Fast broadband inversion by adiabatic pulses. J Magn Reson. 1998;133(1):200–203. [PubMed]

24. Wang J, Mao W, Qiu M, Smith MB, Constable RT. Factors influencing flip angle mapping in MRI: RF pulse shape, slice-select gradients, off-resonance excitation, and B0 inhomogeneities. Magn Reson Med. 2006;56:463–468. [PubMed]

25. Hua J, Jones CK, Blakely J, Smith SA, van Zijl PC, Zhou J. Quantitative description of the asymmetry in magnetization transfer effects around the water resonance in the human brain. Magn Reson Med. 2007;58(4):786–793. [PubMed]

26. Wang J, Qiu M, Constable RT. In vivo method for correcting transmit/receive nonuniformities with phased array coils. Magn Reson Med. 2005;53:666–674. [PubMed]